Journal of Rare Earths 38 (2020) 883–890

Contents lists available at ScienceDirect

Journal of Rare Earths

journal homepage: http://www.journals.elsevier.com/journal-of-rare-earths

Influence of CeO_2 loading on structure and catalytic activity for NH_3-SCR over TiO_2-supported CeO_2☆

Hongliang Zhang [a, b, c], Long Ding [a], Hongming Long [a, b, ***], Jiaxin Li [a, b], Wei Tan [d], Jiawei Ji [d], Jingfang Sun [d], Changjin Tang [d, **], Lin Dong [d, *]

[a] School of Metallurgical Engineering, Anhui University of Technology, Ma'anshan 243032, China
[b] Key Laboratory of Metallurgical Emission Reduction & Resources Recycling (Anhui University of Technology), Ministry of Education, Ma'anshan 243002, China
[c] Analysis and Testing Central Facility, Anhui University of Technology, Ma'anshan 243002, China
[d] Jiangsu Key Laboratory of Vehicle Emissions Control, School of Chemistry and Chemical Engineering, Nanjing University, Nanjing 210093, China

ARTICLE INFO

Article history:
Received 30 October 2019
Received in revised form
7 January 2020
Accepted 8 January 2020
Available online 13 January 2020

Keywords:
CeO_2
Selective catalytic reduction
Redox property
Dispersion capacity
Structure–activity relationship
Rare earths

ABSTRACT

A series of supported CeO_2/TiO_2 catalysts were prepared to explore the influence of CeO_2 loading on these catalysts for the selective catalytic reduction of NO_x by NH_3 (NH_3-SCR). The catalysts were investigated in detail by means of XRD, Raman, H_2-TPR, NH_3-TPD, XPS, *in situ* DRIFTS, and NH_3-SCR reaction. The activity of the catalyst is closely related to the content of CeO_2. When the loading of CeO_2 is near the dispersion capacity (1.16 mmol Ce^{4+}/100 m^2 TiO_2), the catalytic activity is better. This may be because that the dispersed CeO_2 is the active species and the catalyst has appropriate redox property, along with the larger amounts of surface Ce content and surface adsorbed oxygen species. Finally, a possible reaction mechanism via the Langmuir-Hinshelwood (L-H) mechanism is tentatively proposed to further understand the NH_3-SCR reaction.

1. Introduction

Nitrogen oxides (NO_x) cause photochemical smog, ozone depletion and acid rain, which seriously threaten the ecological environment and human health.[1] Many rigorous environmental regulations have been put forward all over the world to control the emission of NO_x from mobile sources (e.g. motor vehicles) and staionary sources (e.g. coal-fired power plants). The selective catalytic reduction of NO_x by NH_3 (NH_3-SCR) is an efficient denitration technology, which is widely used for the abatement of nitrogen oxides from power plants.[2] V_2O_5-WO_3 (MoO_3) catalysts supported on TiO_2 are the most widely used catalysts, because they have high denitration efficiency and good sulfur resistance at 300–400°C. Nevertheless, V_2O_5-WO_3 (MoO_3)/TiO_2 catalyst will gradually be replaced due to the toxicity of vanadium species, poor N_2 selectivity at higher temperatures and narrow operation temperature window.[3]

At present, the research of vanadium-free SCR catalysts mainly focuses on rare earth metal and transition metal catalysts, including iron, copper, manganese and cerium-based catalysts.[4–7] Among these catalysts, ceria (CeO_2) has been extensively investigated owing to its preferable oxygen storage and good redox performance associated with the capability of efficiently transferring the electron in Ce^{3+}/Ce^{4+}, which is a key function to eliminate NO_x.[8–10] The NH_3-SCR reactivity of pure CeO_2 is poor, but its catalytic performance can be significantly improved when it was prepared into supported ceria-based catalysts[11–14] or by the introduction of acidic materials for the improvement of surface acidity.[15,16] TiO_2 is widely used as supports of ceria-based SCR catalysts for its superior sulfur resistance.[17–19] TiO_2 not only is inert material for supported metal-oxide catalysts, but also has significant effects on the catalytic and

☆ **Foundation item:** Project supported by the National Natural Science Foundation of China (21773106, 21677069, 51674002, 21307001), and the Open Project Program of Jiangsu Key Laboratory of Vehicle Emissions Control (OVEC037).
* Corresponding author.
** Corresponding author.
*** Corresponding author. School of Metallurgical Engineering, Anhui University of Technology, Ma'anshan 243032, China.
E-mail addresses: yaflhm@126.com (H.M. Long), tangcj@nju.edu.cn (C.J. Tang), donglin@nju.edu.cn (L. Dong).

https://doi.org/10.1016/j.jre.2020.01.005
1002-0721/

physicochemical properties of the active components. Therefore, it is necessary to investigate the interaction between supports (TiO_2) and components (CeO_2). However, the relationship between "composition-structure-property" of CeO_2/TiO_2 catalysts is still not very clear.

In this work, TiO_2 was applied as support to synthesize CeO_2/TiO_2 catalysts with different CeO_2 loading amounts. X-ray diffraction (XRD), Raman spectroscopy, H_2-temperature programmed reduction (H_2-TPR), NH_3-temperature programmed desorption (NH_3-TPD), and X-ray photoelectron spectroscopy (XPS) were applied to investigate the physicochemical properties of CeO_2/TiO_2 catalysts. The SCR catalytic properties of these samples were evaluated to comprehend the relationship between the structure and SCR performance of CeO_2/TiO_2 catalysts. Then, we investigated the interaction of NH_3 and NO + O_2 with CeO_2/TiO_2 by *in situ* diffuse reflectance Fourier-transformed infrared spectroscopy (*in situ* DRIFTS) to discuss the reaction mechanism of NH_3-SCR over CeO_2/TiO_2 catalysts.

2. Experimental

2.1. Catalysts preparation

CeO_2/TiO_2 catalysts with various CeO_2 contents were synthesized by the impregnation method. Firstly, TiO_2 (67 m^2/g) was immersed into $Ce(NO_3)_3$ solution, stirred for 1 h at room temperature, and then evaporated at 100 °C. The obtained residue was dried at 105 °C overnight, and finally in air stream calcined at 450 °C for 5 h. The samples were labeled as *x*CeTi. For example, 06CeTi means a sample with CeO_2 loading amount of 0.6 mmol CeO_2/100 m^2 TiO_2.

2.2. Catalysts characterization

XRD measurements were carried out on a Philips X'pert Pro diffractometer using Cu Kα (40 kV, 40 mA) radiation. The 2θ angles were collected over a range of 10° – 80° at a scan speed of 10(°) /min.

Raman spectrum was measured on a Renishaw inVia Reflex Laser Raman spectrometer using a laser with 532 nm wavelength.

H_2-TPR was carried out on a fixed reaction bed connected to a thermal conductivity detector (TCD). About 50 mg catalyst was outgassed at 100 °C for 1 h in a N_2 stream. TPR was performed from 50 to 800 °C at 10 °C/min with Ar-H_2 mixture.

NH_3-TPD was performed on a fixed reaction bed. About 100 mg catalyst was outgassed at 100 °C in air for 1 h. Then the catalysts absorbed pure NH_3 at 100 °C for 0.5 h and subsequently by N_2 purging for 1 h. The samples were carried out from 100 to 500 °C at 10 °C/min in pure He.

XPS was performed on a PHI 5000 VersaProbe system by setting the adventitious C 1s peak located at 284.8 eV as the reference.

In situ DRIFTS was collected at a resolution of 4 cm^{-1} from 4000 to 650 cm^{-1} via accumulating 32 scans on an FT-IR spectrometer (Nicolet 5700) fitted out with Harrick DRIFTS cell and high-sensitive MCT detector cooled.

2.3. Catalytic performance measurements

The NH_3-SCR reaction was evaluated in a quartz stationary bed reactor. The reaction was conducted with a gas hourly space velocity of 120000 mL/(g·h), involving a reaction gas composition composed of 500 ppm NO, 500 ppm NH_3, 5% O_2, and N_2 in balance. The concentrations NO and NO_2 of entrance and exit were monitored by an ECOM J2KN flue gas analyzer. Finally, NO conversion was calculated by the following equation:

$$NO_x\ \text{conversion} = \frac{[NO]_{in} + [NO_2]_{in} - [NO]_{out} - [NO_2]_{out}}{[NO]_{in} + [NO_2]_{in}} \times 100\% \quad (1)$$

3. Results and discussion

3.1. Catalytic test results

Fig. 1 shows the NO conversion over CeO_2/TiO_2 catalysts with various CeO_2 contents at different temperatures. The conversion of NO increases with the reaction temperature. The SCR catalytic activity of pure TiO_2 and CeO_2 samples is relatively low. For example, the NO conversion is only 20% for pure CeO_2 at 450 °C. When CeO_2 is loaded on TiO_2, the SCR activity of these catalysts increases significantly. This is owing to the interaction between TiO_2 and CeO_2, which effectively regulates the redox properties and surface acidity of the catalysts, and thus greatly improving the catalytic performance. The CeO_2 loading amount has a great impact on the activity of these catalysts: when the CeO_2 loading amount increases from 0.3 to 1.2 mmol CeO_2/100 m^2 TiO_2, the catalytic activity increases obviously at various reaction temperatures; and when the CeO_2 loading amount increases from 1.2 to 2.8 mmol CeO_2/100 m^2 TiO_2, the activity of these catalysts does not increase significantly. Therefore, SCR activity of supported CeO_2/TiO_2 is closely related to the loading (or dispersion) of CeO_2, and there is an optimum loading (e.g. 12CeTi). Fig. S1 indicates that the N_2 selectivity of CeO_2/TiO_2 is more than 95% at all of the temperatures.

The actual working conditions of coal fired power plants usually contain certain amounts of SO_2; thus it is necessary to investigate the influence of SO_2 on SCR activities of catalysts. Fig. S2 shows the results of catalytic activity in the presence of SO_2 over 12CeTi. NO conversion declines continuously from *ca.* 70% to *ca.* 30% during the whole testing for 12CeTi, which is because sulfates adsorb on the loaded CeO_2 to form metal sulfates and block the active site of Ce–O–Ti, resulting in the irreversible deactivation of the catalysts.

3.2. Structural characteristics (XRD and Raman)

XRD can determine the crystal structure of TiO_2 and the dispersion behavior of CeO_2, and the corresponding results are given in Fig. 2(a). According to PDF-ICDD 21-1272, a series of

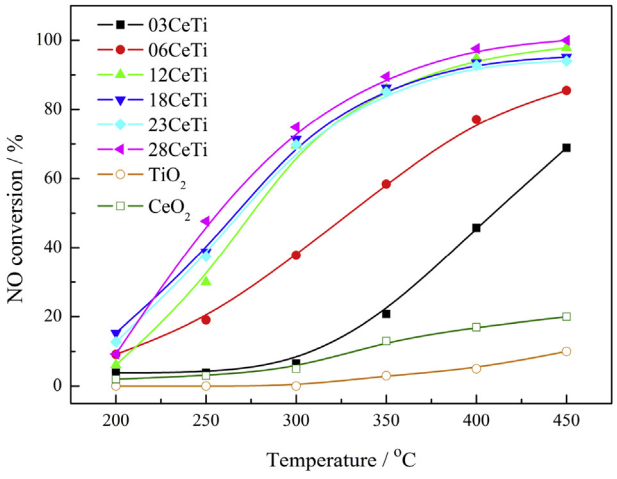

Fig. 1. SCR performance of CeO_2/TiO_2 catalysts with various CeO_2 contents.

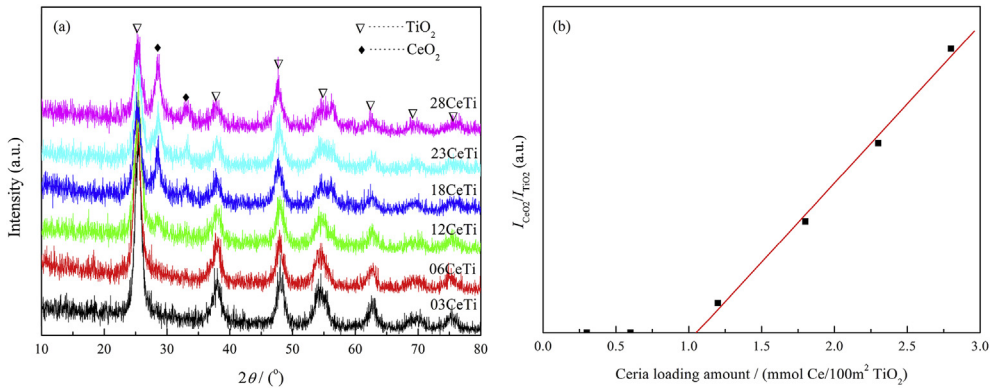

Fig. 2. XRD patterns (a) and the quantitative XRD results (b) of the CeO_2/TiO_2 samples.

diffraction peaks at 25.30°, 37.93°, 48.42°, 54.30°, 62.79°, 69.45° and 75.54° are ascribed to anatase TiO_2; according to PDF-ICDD 34-0394, the diffraction peaks at 28.58° and 33.09° are ascribed to cubic fluorite-type CeO_2. For CeO_2/TiO_2 samples, the characteristic diffraction peaks of TiO_2 gradually weaken with the increase of CeO_2 content, which may be due to the weakening of the X-ray diffraction of TiO_2 by the CeO_2 loading on the TiO_2 surface, or the disordering of TiO_2 caused by the introduction of CeO_2.[20] No diffraction peaks of CeO_2 were detected for samples with low ceria content (<1.2 mmol CeO_2/100 m^2 TiO_2), which suggests that CeO_2 is highly dispersed on the TiO_2 surface. When the content of CeO_2 is up to 1.2 mmol CeO_2/100 m^2 TiO_2, the diffraction peaks of crystal CeO_2 appear at 28.58° and 33.09°, and the peak intensity increases with the CeO_2 loading content.

In order to further determine the dispersion capacity of CeO_2 on the support TiO_2 surface, the X-ray diffraction quantitative analysis was carried out by calculating the ratio of the main diffraction peak intensity between crystal CeO_2 and TiO_2 support as a function of the loading content of CeO_2. As shown in Fig. 2(b), we can calculate that the straight line does not pass through the origin, but has an intercept on the *x*-axis, which corresponds to the dispersion capacity of CeO_2 on the support TiO_2 surface. XRD quantitative results demonstrate that the dispersion capacity of CeO_2 on the support TiO_2 surface is about 1.05 mmol/100 m^2 TiO_2. The dispersion capacity shows that CeO_2 in a dispersed form exists on the support TiO_2 surface when the loading of CeO_2 is less than 1.05 mmol/100 m^2 TiO_2. When the loading of CeO_2 exceeds 1.05 mmol/100 m^2 TiO_2, CeO_2 exists not only in a dispersed form, but also in some crystalline forms on the support. In order to enhance the persuasiveness of the data, the samples were characterized by Raman spectra as a supplementary measurement of XRD. As shown in Fig. 3(a), the peaks at 397, 517 and 639 cm^{-1} correspond to $B_{1g(1)}$, A_{1g} + $B_{1g(2)}$ and $E_{g(3)}$ vibration modes of anatase TiO_2, respectively.[21] The Raman peak at 461 cm^{-1} is attributed to the F_{2g} vibration modes of cubic fluorite-type CeO_2.[22,23] Raman peaks of crystalline CeO_2 were not detected for samples with CeO_2 content less than 1.2 mmol/100 m^2 TiO_2, which indicates that CeO_2 is highly dispersed on the surface of TiO_2. When the loading of CeO_2 is more than 1.2 mmol/100 m^2 TiO_2, Raman peaks of crystalline CeO_2 appear, which is the same as XRD results. A similar method was used for Raman quantitative analysis and the results are shown in Fig. 3(b). When the dispersion capacity of CeO_2 on the support TiO_2 surface is about 1.04 mmol/100 m^2 TiO_2, the value of CeO_2 is approximately the same as that obtained by XRD quantitative analysis.

According to the literature, anatase TiO_2 with a deformed NaCl structure belongs to tetragonal system ($a = b \neq c$, $\alpha = \beta = \gamma = 90°$). To investigate the exposed plane of support TiO_2, the HRTEM image is presented in Fig. S3. The periodic fringes (0.24 nm) can be observed, which is compatible with the distance expected between the (001) reticular planes of anatase TiO_2, hence (001) plane is its preferentially exposed plane,[24] as shown in Fig. 4. The (001) plane of anatase has the octahedral vacant sites available. The area of the constitutional unit can be calculated as follows: $S = a \cdot b = a^2$. According to literature,[25] the lattice parameters of titanium dioxide are $a = b = 0.37852$ nm, and $c = 0.95139$ nm. Every unit mesh can accommodate one Ce^{4+}. Therefore, according to the "Incorporation Model",[26] the theoretical dispersion capacity (DC) of CeO_2 on the support TiO_2 surface can be calculated as follows: $DC = \frac{100m^2}{6.02\times10^{23}a^2} \approx 1.16$ mmol Ce^{4+}/100 m^2 TiO_2. This result matches the experimental results well. When the content of CeO_2 is below this value, the dispersed Ce^{4+} ions can be incorporated into

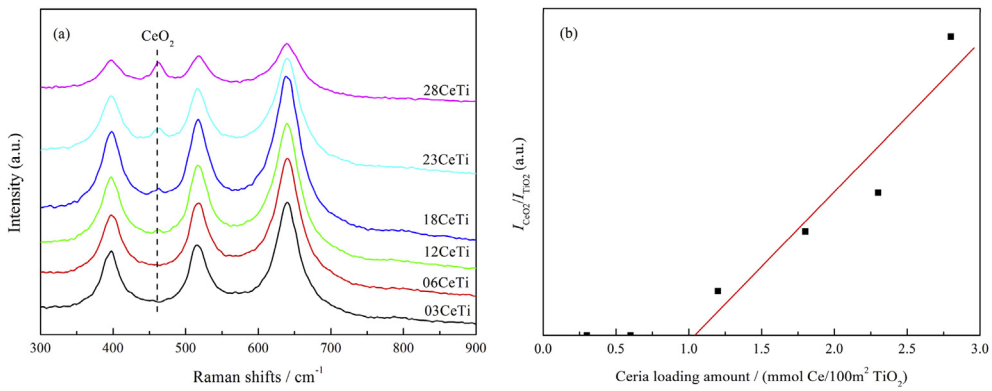

Fig. 3. Raman spectra (a) and the quantitative Raman results (b) over the CeO_2/TiO_2 catalysts.

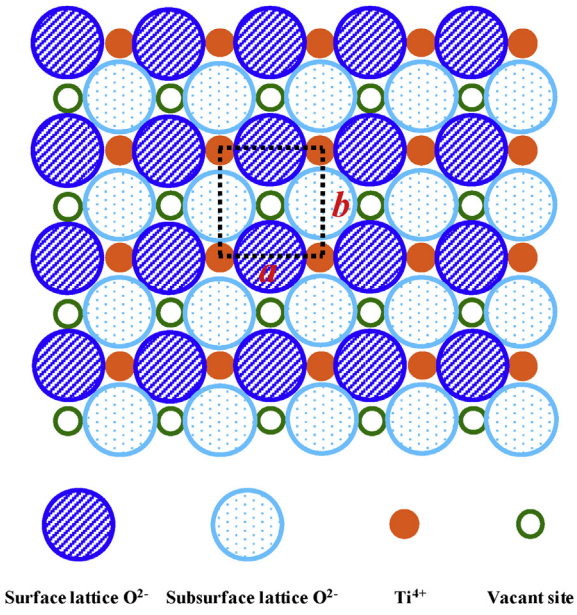

Fig. 4. The schematic diagram of the (001) crystal plane of TiO_2 support.

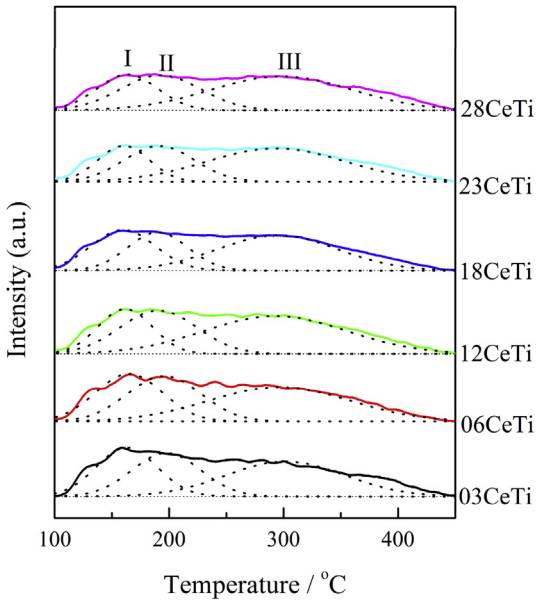

Fig. 6. NH_3-TPD profiles of the CeO_2/TiO_2 samples with various CeO_2 contents.

these vacant positions and the corresponding O^{2-} ions will be located at the top for charge compensation. When the CeO_2 content is more than its dispersion capacity, the highly dispersed CeO_2 will occupy all the vacancies and the crystalline CeO_2 can be detected.

As we all know, supported catalysts with active component loading near the dispersion capacity exhibit the best catalytic behavior in heterogeneous catalysis. Combining with the results of catalytic activity, it can be seen that the dispersion behavior of CeO_2 has a great influence on SCR activity: dispersed CeO_2 is more favorable for SCR reactivity on CeO_2/TiO_2, and when the loading of CeO_2 is close to the dispersion capacity (e.g. 12CeTi), the catalytic activity of samples reaches the optimum; while crystalline CeO_2 has relatively little impact on the catalytic activity of CeO_2/TiO_2. It is obvious that the catalytic activity of the samples has little change when the loading of CeO_2 exceeds the dispersion capacity.

3.3. Reduction properties (H_2-TPR)

It is of great significance to NH_3-SCR reaction that the catalyst has appropriate redox ability to activate NH_3 molecule. H_2-TPR technology was used to characterize the redox performance of these samples, and the results are shown in Fig. 5. H_2-TPR curves of CeO_2/TiO_2 catalysts with various CeO_2 contents are similar to each other, showing two broad reduction peaks in 590–660 °C (α peak) and 620–680 °C (β peak), respectively. The reduction peak α can be ascribed to the reduction of surface oxygen, while the reduction peak β is ascribed to the reduction of Ce–O–Ti species, which generates from the interaction between CeO_2 and TiO_2.[18,27] Along with the increasing CeO_2 content, the peak area of reduction peaks increases and the reduction temperature decreases, which indicates that CeO_2

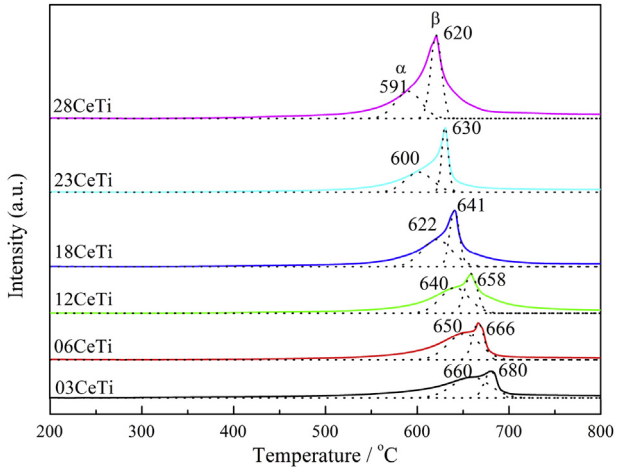

Fig. 5. H_2-TPR profiles of the CeO_2/TiO_2 samples with various CeO_2 contents.

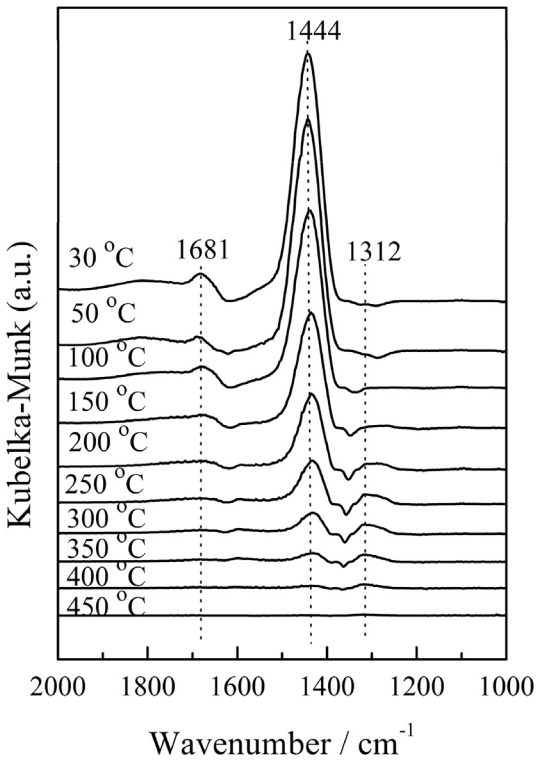

Fig. 7. NH_3-desorption *in situ* DRIFTS of the representative catalyst (12CeTi).

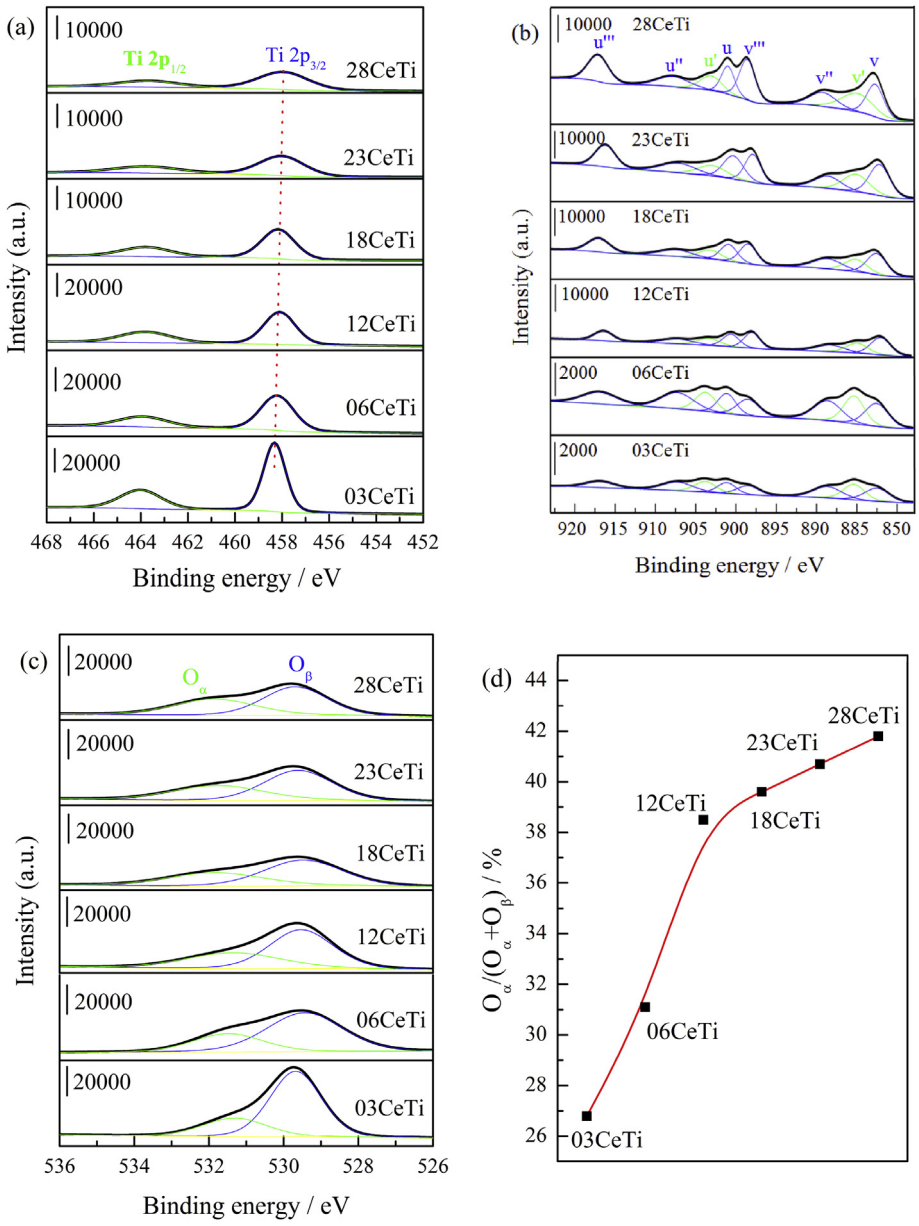

Fig. 8. XPS spectra of Ti 2p (a), Ce 3d (b) and O 1s (c) of the catalysts; (d) The relative concentrations of surface-adsorbed oxygen ($O_\alpha/(O_\alpha+O_\beta)$).

increases the content of surface oxygen and promotes the reduction of surface oxygen. According to the previous researches,[13,28,29] the improvement of redox performance of catalysts can benefit oxygen migration, for instance, the transfer of lattice oxygen in CeO_2 to form surface oxygen which can be easily reduced to produce oxygen vacancies, and then accelerate the generation of chemisorbed oxygen on the surface. It is well known that surface chemisorbed oxygen can effectively oxidize NO to NO_2, thus via the "fast SCR" approach enhancing the catalytic reactions. Of course, too high redox ability may lead to unselective oxidation of NH_3 thus resulting in the lack of reducing agents and poor N_2 selectivity.

3.4. Surface acidities (NH_3-TPD and NH_3-desorption in situ DRIFTS)

NH_3-TPD can be used for determining surface acid sites of these samples. In Fig. 6, three NH_3 desorption bands can be observed in a wide temperature range, which are labeled as I, II and III. The desorption band I at low temperature is considered to be the desorption of weakly adsorbed ammonia; the desorption band II at medium temperature is related to the desorption of moderately strong chemisorbed ammonia; and the desorption peak III at high temperature is ascribed to the desorption of strong chemisorbed ammonia.[30,31] Weakly adsorbed adsorption (peak I) is unable to activate ammonia molecule, while NH_3 adsorption on moderately strong and strong acid sites (peak II and peak III) contributes more to NH_3-SCR reaction. With the increase of CeO_2 loading, the peak area changes little, which indicates that CeO_2 has less influence on the acidity of the catalysts. This is because the acidity of CeO_2/TiO_2 is mainly caused by TiO_2.

For the sake of clarifying the types of acid sites of the catalysts and the change of adsorbed ammonia species during the heating process, NH_3-desorption *in situ* DRIFTS experiments were carried out on the representative sample (12CeTi), as shown in Fig. 7. According to the literature,[32–34] the peaks at 1140–1240 cm^{-1} and 1580–1610 cm^{-1}

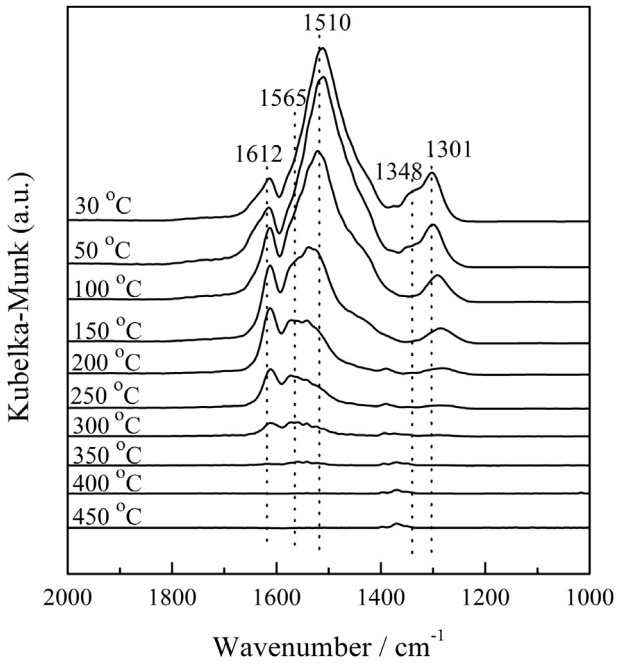

Fig. 9. *In situ* DRIFTS of NO + O_2 adsorption on 12CeTi catalyst.

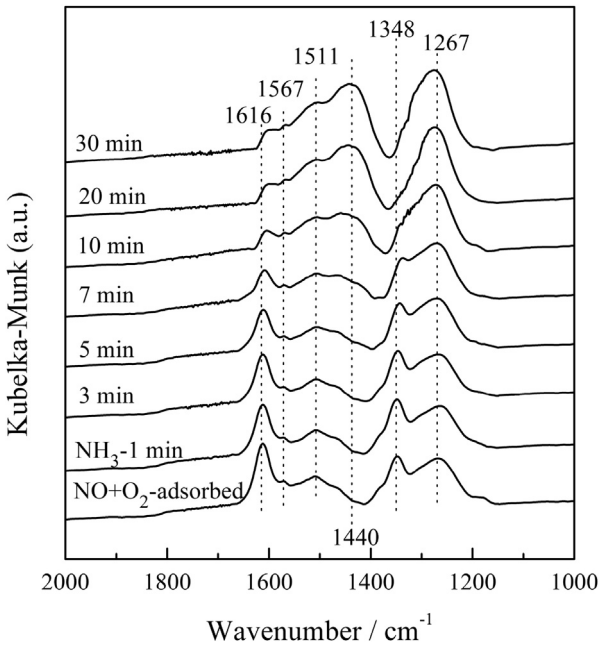

Fig. 11. *In situ* DRIFTS over 12CeTi at 250 °C between NH_3 and pre-adsorbed NO_x species as a function of time.

belong to the IR vibration characteristic peaks of NH_3 adsorbed on Lewis (L) acid sites, while those at 1415–1465 cm^{-1} and 1670–1695 cm^{-1} belong to the IR vibration characteristic peaks of NH_4^+ adsorbed on Brønsted (B) acid site. The adsorbed ammonia species is involved in SCR process and reacts with the adsorbed NO_x species to form an active intermediate.[35] For 12CeTi catalyst (Fig. 7), when ammonia-nitrogen mixed gas is introduced at room temperature, ammonia is adsorbed on the 12CeTi catalyst surface. IR vibration peaks are generated at 1681 and 1444 cm^{-1}, mainly attributed to the characteristic peaks of NH_4^+ adsorbed on B acid site, but NH_3 adsorbed on L acid site is not found. Therefore, only NH_4^+ is involved in SCR process for CeO_2/TiO_2 catalyst, so the desorption peak of NH_3-TPD is mainly NH_4^+ on B acid site. As the temperature increases, the vibration peak of the adsorbed species on the B acid site gradually weakens until it disappears; when the sample is heated to 150 °C, a new vibration peak emerges at 1312 cm^{-1} attributed to $-NH_2$ species. This indicates that with the increase of temperature, dehydrogenation of NH_4^+ transforms into $-NH_2$ species which then participates in SCR reaction.

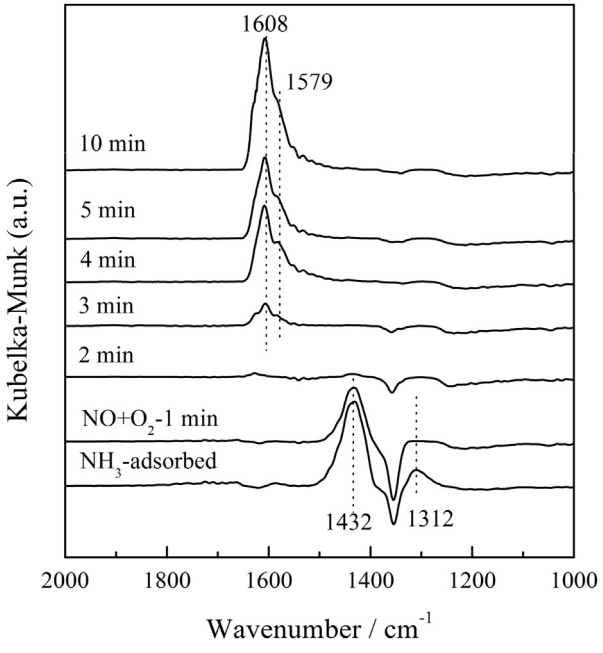

Fig. 10. *In situ* DRIFTS over 12CeTi at 250 °C between NO + O_2 and pre-adsorbed NH_3 species as a function of time.

3.5. Surface analysis (XPS)

XPS was selected to study the chemical state and surface properties of CeO_2/TiO_2 catalysts. For Ti 2p XPS spectra in Fig. 8(a), the main peak at low binding energy is assigned to Ti $2p_{3/2}$, and the secondary peak at high binding energy is assigned to Ti $2p_{1/2}$. With the increase of CeO_2 loading amount, the intensity of Ti 2p peak gradually weakens, which is due to the fact that CeO_2 covers the surface of TiO_2. Meanwhile, the binding energy of Ti $2p_{3/2}$ shifts to low binding energy (458.4 eV → 458.0 eV) with the increase of CeO_2 loading amount. This is because Ce^{3+}-□-Ti^{3+} (□ stands for oxygen vacancies) can be formed by oxygen release of the formed Ce—O—Ti structure, thereby increasing the electron cloud density of Ti^{4+}.

For Ce 3d XPS spectra in Fig. 8(b), Ce 3d of all catalysts can be divided into $3d_{3/2}$ and $3d_{5/2}$ peaks (marked as u and v, respectively)

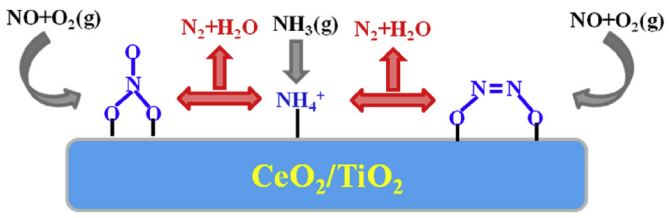

Fig. 12. Possible reaction mechanism of CeO_2/TiO_2 catalyst at 250 °C.

due to spin-orbital multiplets, and fitted with eight peaks by Gaussian-Lorentz. Among them, the peaks marked as u' and v' represent the $3d^{10}4f^1$ electronic state of Ce^{3+}, and the other six bands correspond to the $3d^{10}4f^0$ electronic state of Ce^{4+}.[36–38] The intensities of Ce 3d spectra increase with the CeO_2 loading amount. In addition, Ce^{4+} and Ce^{3+} coexist in CeO_2/TiO_2 samples. The conversion between Ce^{3+} and Ce^{4+} can accelerate the generation of oxygen vacancies: $4Ce^{4+} + O^{2-} \rightarrow 4Ce^{4+} + 2e^-/\square + 0.5O_2 \rightarrow 2Ce^{4+} + 2Ce^{3+} + \square + 0.5O_2$ ($\square$ stands for vacancies); the generation of oxygen vacancies is conducive to the dissociation of NO molecule and further improves the catalytic performance of NH_3-SCR reaction.

For O 1s XPS spectra in Fig. 8(c), the XPS spectra of O 1s are fitted into two peaks. The main peak at low binding energy (529.6 eV) labeled as O_β is assigned to lattice oxygen species (O^{2-}). The high binding energy (531.8 eV) labeled as O_α is assigned to surface adsorbed oxygen species (O_2^{2-} or O^- ascribed to defect-oxide or hydroxyl-like group).[39] The relative content of surface adsorbed oxygen specie can be estimated by the peak area ratio of O_α and $O_\alpha+O_\beta$ (i.e. $O_\alpha/(O_\alpha+O_\beta)$). As listed in Fig. 8(d), when the CeO_2 loading amount is less than 1.2 mmol CeO_2/100 m^2 TiO_2, the amount of surface adsorbed oxygen species increases rapidly with the CeO_2 loading; when the CeO_2 loading amount exceeds 1.2 mmol CeO_2/100 m^2 TiO_2, the amount of surface adsorbed oxygen specie increases slowly with the CeO_2 loading. The surface adsorbed oxygen has higher mobility than lattice oxygen, so they have higher activity than lattice oxygen, which is more conducive to NO oxidation to NO_2 and then promotes the "fast SCR" approach.[40,41] In addition, with the increase of CeO_2 loading, a large number of surface hydroxyl groups were formed on the surface of the catalyst. They adsorbed NH_3 at B acid sites and formed NH_4^+, which reacts with adsorbed nitrogen oxides such as NO_2 to form N_2 and H_2O.[42]

3.6. In situ DRIFTs studies between catalysts and reactants

The NO + O_2 co-adsorption *in situ* DRIFTS of 12CeTi sample is presented to study the adsorption behavior of nitrogen oxides, as shown in Fig. 9. For 12CeTi catalyst, a series of vibration peaks ascribed to the types of adsorbed NO_x can be detected at room temperature from 1000 to 2000 cm^{-1}: bridged nitrate (1612 cm^{-1}), bidentate nitrate (1565 cm^{-1}), monodentate nitrate (1510 cm^{-1}), monodentate nitrite (1301 cm^{-1})[43–45]; the band at 1348 cm^{-1} corresponds to *cis*-$N_2O_2^{2-}$ formed when two NO molecules are adsorbed on the surface oxygen vacancies, and reaction activity is very high.[46] With the increase of temperature, adsorbed nitrogen oxides gradually disappear due to transformation/decomposition/desorption.

In order to study whether the adsorbed ammonia species could react with NO + O_2, the catalyst was pretreated with NH_3 for 30 min, then purged with N_2 at 250 °C to remove the weakly adsorbed NH_3, and finally treated with NO + O_2 gas mixture. The obtained spectra are shown in Fig. 10. When NH_3 is saturated at 250 °C, signals of B acid (1432 and 1312 cm^{-1}) can be observed. Then, the NH_3 gas is shut down and the mixture of NO + O_2 is introduced. Some interesting behaviours could be discovered as below: (1) the signals related to NH_3 adsorption disappear rapidly after NO + O_2 mixture is introduced for 2 min; (2) bridged nitrate (1608 cm^{-1}) and bidentate nitrate (1579 cm^{-1}) appear at 3 min, and then increase to stable state for 10 min. The results show that NH_3 species adsorbed to B acid sites participate in SCR process on 12CeTi catalyst.

In order to study whether the adsorbed NO_x species could react with NH_3, the catalyst was pretreated with NO + O_2 mixture for 30 min, then purged with N_2 at 250 °C to remove the weakly adsorbed NO_x, and finally treated with NH_3 gas. The obtained spectra are shown in Fig. 11. When NO + O_2 is saturated at 250 °C, the signals of bridged nitrate (1616 cm^{-1}), bidentate nitrate (1567 cm^{-1}), monodentate nitrate (1511 cm^{-1}), *cis*-$N_2O_2^{2-}$ (1348 cm^{-1}) and monodentate nitrite (1267 cm^{-1}) can be observed. Then, turn off NO + O_2 gas and introduce NH_3 gas. When the NH_3 gas is introduced, the species of bridged nitrate and *cis*-$N_2O_2^{2-}$ decrease gradually, while the species of bidentate nitrate, monodentate nitrate and monodentate nitrite do not change significantly; meanwhile, the peak of adsorbed NH_3 species (1440 cm^{-1}) increases gradually. The results show bridged nitrates and *cis*-$N_2O_2^{2-}$ species are more likely to react with NH_3.

We also characterized the catalysts with low CeO_2 loading (03CeTi) and with high CeO_2 loading (18CeTi) by *in situ* DRIFTS shown in Figs. S4 and S5, and found that their reaction process was similar to that of 12CeTi catalyst. Based on the characterization results of *in situ* DRIFTS, the possible reaction mechanism of the catalysts at 250 °C is proposed (Fig. 12). Firstly, NO molecules are oxidized or activated at the active sites such as oxygen vacancies to form bridged nitrates and *cis*-$N_2O_2^{2-}$. Secondly, N_2 and H_2O are formed by the reaction of the absorbed NO_x with NH_4^+ at the B acid site, which conforms to the Langmuir-Hinshelwood (L-H) reaction mechanism.

4. Conclusions

A series of CeO_2/TiO_2 catalysts were prepared by impregnation with TiO_2 as support. The relationship between catalyst structure, dispersion, reducibility, acidity, adsorption and SCR catalytic performance was systematically studied. Based on the above characterization results, the following conclusions can be drawn: (1) The experimental value of the dispersion capacity of CeO_2 on TiO_2 is about 1.05 mmol Ce^{4+}/100 m^2 TiO_2, which is close to the predicted value of the "Incorporation Model" (1.16 mmol Ce^{4+}/100 m^2 TiO_2). (2) The activity of the catalyst is closely bound up with the loading of CeO_2. When the loading is lower than the dispersion capacity, the activity of the catalyst increases obviously with the loading amount increasing. When CeO_2 exceeds the dispersion capacity, the activity of catalyst does not change significantly with the increase of loading. (3) As CeO_2 loading increases, on the one hand, the amount of surface oxygen is increased; on the other hand, surface oxygen can be easily reduced to generate oxygen vacancies, which promote the generation of chemisorbed oxygen species on the surface. Surface-chemisorbed oxygen species effectively oxidize NO to NO_2, thereby accelerating catalytic activity via the "fast NH_3-SCR" approach. (4) Based on the characterization results of *in situ* DRIFTS, NH_3 molecule is mainly activated at the B acid site, and reacts with the adsorbed NO_x species (such as bridged nitrate, *cis*-$N_2O_2^{2-}$) to produce N_2 and H_2O, which conforms to the L-H reaction mechanism.

Appendix A. Supplementary data

Supplementary data to this article can be found online at https://doi.org/10.1016/j.jre.2020.01.005.

References

1. Chen L, Wang D, Wang JD, Weng D, Cao L. Hydrothermal and sulfur aging of CeTi/CeWTi catalysts for selective catalytic reduction of NO_x with NH_3. *J Rare Earths*. 2019;37:829.
2. Yang B, Huang Q, Chen MD, Shen YS, Zhu SM. Mn-Ce-Nb-O_x/P84 catalytic filters prepared by a novel method for simultaneous removal of particulates and NO. *J Rare Earths*. 2019;37:273.
3. Ma L, Seo CY, Nahata M, Chen XY, Li JH, Schwank JW. Shape dependence and sulfate promotion of CeO_2 for selective catalytic reduction of NO_x with NH_3. *Appl Catal, B*. 2018;232:246.

4. Yan LJ, Gu YD, Han LP, Wang PL, Li HR, Yan TT, et al. Dual promotional effects of TiO_2-decorated acid-treated MnO_x octahedral molecular sieve catalysts for alkali-resistant reduction of NO_x. *ACS Appl Mater Interfaces*. 2019;11:11507.
5. Chen YX, Li C, Chen JX, Tang XF. Self-prevention of well-defined-facet Fe_2O_3/MoO_3 against deposition of ammonium bisulfate in low-temperature NH_3-SCR. *Environ Sci Technol*. 2018;52:11796.
6. Ma JW, Li YH, Liu J, Zhao Z, Xu CM, Wei YC, et al. Cu-SAPO-18 for NH_3-SCR reaction: the effect of different aging temperatures on Cu^{2+} active sites and catalytic performances. *Ind Eng Chem Res*. 2019;58:2389.
7. Liu K, He H, Yu YB, Yan ZD, Yang WW, Shan WP. Quantitative study of the NH_3-SCR pathway and the active site distribution over $CeWO_x$ at low temperatures. *J Catal*. 2019;369:372.
8. Yao WY, Wang XQ, Liu Y, Wu ZB. Ce-O-P material supported CeO_2 catalysts: a novel catalyst for selective catalytic reduction of NO with NH_3 at low temperature. *Appl Surf Sci*. 2019;467–468:439.
9. Liu S, Feng X, Liu JY, Lin QJ, Xiong L, Wang Y, et al. Investigation of the selective catalytic reduction of NO with NH_3 over the $WO_3/Ce_{0.68}Zr_{0.32}O_2$ catalyst: the role of H_2O in SO_2 inhibition. *New J Chem*. 2019;43:2258.
10. Lian ZH, Shan WP, Zhang Y, Wang M, He H. Morphology-dependent catalytic performance of NbO_x/CeO_2 catalysts for selective catalytic reduction of NO_x with NH_3. *Ind Eng Chem Res*. 2018;57:12736.
11. Chen JX, Chen YX, Zhou MJ, Huang ZW, Gao JY, Ma Z, et al. Enhanced performance of ceria-based NO_x reduction catalysts by optimal support effect. *Environ Sci Technol*. 2017;51:473.
12. Shen YS, Zhu SM, Qiu T, Shen SB. A novel catalyst of CeO_2/Al_2O_3 for selective catalytic reduction of NO by NH_3. *Catal Commun*. 2009;11:20.
13. Yao XJ, Chen L, Kong TT, Ding SM, Luo Q, Yang FM. Support effect of the supported ceria-based catalysts during NH_3-SCR reaction. *Chin J Catal*. 2017;38:1423.
14. Fang C, Zhang DS, Shi LY, Gao RH, Li HR, Ye LP, et al. Highly dispersed CeO_2 on carbon nanotubes for selective catalytic reduction of NO with NH_3. *Catal Sci Technol*. 2013;3:803.
15. Song ZX, Zhang QL, Ma YX, Liu QX, Ning P, Liu X, et al. Mechanism-dependent on the different CeO_2 supports of phosphotungstic acid modification CeO_2 catalysts for the selective catalytic reduction of NO with NH_3. *J Taiwan Inst Chem Eng*. 2017;71:277.
16. Song ZX, Zhang QL, Ning P, Fan J, Duan YK, Liu X, et al. Effect of CeO_2 support on the selective catalytic reduction of NO with NH_3 over P-W/CeO_2. *J Taiwan Inst Chem Eng*. 2016;65:149.
17. Xu WQ, Yu YB, Zhang CB, He H. Selective catalytic reduction of NO by NH_3 over a Ce/TiO_2 catalyst. *Catal Commun*. 2008;9:1453.
18. Yao XJ, Zhao RD, Chen L, Du J, Tao CY, Yang FM, et al. Selective catalytic reduction of NO_x by NH_3 over CeO_2 supported on TiO_2: comparison of anatase, brookite, and rutile. *Appl Catal, B*. 2017;208:82.
19. Xiao X, Xiong SC, Shi YJ, Shan WP, Yang SJ. Effect of H_2O and SO_2 on the selective catalytic reduction of NO with NH_3 over Ce/TiO_2 catalyst: mechanism and kinetic study. *J Phys Chem C*. 2016;120:1066.
20. Liu LJ, Yu Q, Zhu J, Wan HQ, Sun KQ, Liu B, et al. Effect of MnO_x modification on the adsorption and activity of $CuO/Ce_{0.67}Zr_{0.33}O_2$ catalyst for NO reduction by CO. *J Colloid Interface Sci*. 2010;349:246.
21. Liu ZM, Yi Y, Li JH, Woo SI, Wang BY, Cao XZ, et al. A superior catalyst with dual redox cycles for the selective reduction of NO_x by ammonia. *Chem Commun*. 2013;49:7726.
22. Yao XJ, Gao F, Yu Q, Qi L, Tang CJ, Dong L, et al. NO reduction by CO over CuO-CeO_2 catalysts: effect of preparation methods. *Catal Sci Technol*. 2013;3:1355.
23. Dai QG, Bai SX, Wang ZY, Wang XY, Lu GZ. Catalytic combustion of chlorobenzene over Ru-doped ceria catalysts. *Appl Catal, B*. 2012;126:64.
24. Sun CZ, Zhu J, Lv YY, Qi L, Liu B, Gao F, et al. Dispersion, reduction and catalytic performance of CuO supported on ZrO2-doped TiO2 for NO removal by CO. *Appl Catal, B*. 2011;103:206.
25. Xu BL, Fan YN, Liu L, Lin M, Chen Y. Dispersion state and catalytic properties of vanadia species on the surface of V_2O_5/TiO_2 catalysts. *Sci China, Ser B*. 2002;45:407.
26. Chen Y, Dong L, Jin YS, Xu B, Ji WJ. Studies on supported metal oxide-oxide support interactions (an incorporation model). *Stud Surf Sci Catal*. 1996;101:1293.
27. Liu LJ, Cao Y, Sun W, Yao ZJ, Liu B, Gao F, et al. Morphology and nanosize effects of ceria from different precursors on the activity for NO reduction. *Catal Today*. 2011;175:48.
28. Boningari T, Ettireddy PR, Somogyvari A, Liu Y, Vorontsov A, McDonald CA, et al. Influence of elevated surface texture hydrated titania on Ce-doped Mn/TiO_2 catalysts for the low-temperature SCR of NO_x under oxygen-rich conditions. *J Catal*. 2015;325:145.
29. Chen JF, Zhu JJ, Zhan YY, Lin XY, Cai GH, Wei KM, et al. Characterization and catalytic performance of Cu/CeO2 and Cu/MgO-CeO2 catalysts for NO reduction by CO. *Appl Catal*. 2009;363:208.
30. Zhang DS, Zhang L, Shi LY, Fang C, Li HR, Gao RH, et al. *In situ* supported MnO_x-CeO_x on carbon nanotubes for the low-temperature selective catalytic reduction of NO with NH_3. *Nanoscale*. 2013;5:1127.
31. Fang C, Zhang DS, Cai SX, Zhang L, Huang L, Li HR, et al. Low-temperature selective catalytic reduction of NO with NH_3 over nanoflaky MnO_x on carbon nanotubes *in situ* prepared via a chemical bath deposition route. *Nanoscale*. 2013;5:9199.
32. Liu FD, He H, Zhang CB. Novel iron titanate catalyst for the selective catalytic reduction of NO with NH_3 in the medium temperature range. *Chem Commun*. 2008;17:2043.
33. Peng Y, Li KZ, Li JH. Identification of the active sites on CeO_2-WO_3 catalysts for SCR of NO_x with NH_3: an *in situ* IR and Raman spectroscopy study. *Appl Catal, B*. 2013;140–141:483.
34. Ma L, Cheng YS, Cavataio G, McCabe RW, Fu LX, Li JH. *In situ* DRIFTS and temperature-programmed technology study on NH_3-SCR of NO_x over Cu-SSZ-13 and Cu-SAPO-34 catalysts. *Appl Catal, B*. 2014;156–157:428.
35. Liu FD, He H, Ding Y, Zhang CB. Effect of manganese substitution on the structure and activity of iron titanate catalyst for the selective catalytic reduction of NO with NH_3. *Appl Catal, B*. 2009;93:194.
36. Xie Y, Wu JF, Jing GJ, Zhang H, Zeng SH, Tian XP, et al. Structural origin of high catalytic activity for preferential CO oxidation over CuO/CeO_2 nano catalysts with different shapes. *Appl Catal, B*. 2018;239:665.
37. Li B, Ren ZY, Ma ZX, Huang XD, Liu F, Zhang XB, et al. Selective catalytic reduction of NO by NH_3 over CuO-CeO_2 in the presence of SO_2. *Catal Sci Technol*. 2016;6:1719.
38. Gao FY, Tang XL, Yi HH, Li JY, Zhao SZ, Wang JG, et al. Promotional mechanisms of activity and SO_2 tolerance of Co- or Ni-doped MnO_x-CeO_2 catalysts for SCR of NO_x with NH_3 at low temperature. *Chem Eng J*. 2017;317:20.
39. Bai BY, Arandiyan H, Li JH. Comparison of the performance for oxidation of formaldehyde on nano-Co_3O_4, 2D-Co_3O_4, and 3D-Co_3O_4 catalysts. *Appl Catal, B*. 2013;142–143:677.
40. You XC, Sheng ZY, Yu DQ, Yang L, Xiao X, Wang S. Influence of Mn/Ce ratio on the physicochemical properties and catalytic performance of graphene supported MnO_x-CeO_2 oxides for NH_3-SCR at low temperature. *Appl Surf Sci*. 2017;423:845.
41. Geng Y, Chen XL, Yang SJ, Liu FD, Shan WP. Promotional effects of Ti on a CeO_2-MoO_3 catalyst for the selective catalytic reduction of NO_x with NH_3. *ACS Appl Mater Interfaces*. 2017;9:16951.
42. Wu ZB, Jiang BQ, Liu Y, Wang HQ, Jin RB. DRIFT study of manganese/titania-based catalysts for low-temperature selective catalytic reduction of NO with NH_3. *Environ Sci Technol*. 2007;41:5812.
43. Yang SJ, Guo YF, Chang HZ, Ma L, Peng Y, Qu Z, et al. Novel effect of SO_2 on the SCR reaction over CeO_2: mechanism and significance. *Appl Catal, B*. 2013;136–137:19.
44. Yu Q, Yao X, Zhang HL, Gao F, Dong L. Effect of ZrO_2 addition method on the activity of Al_2O_3-supported CuO for NO reduction with CO: impregnation vs. coprecipitation. *Appl Catal*. 2012;423–424:42.
45. Yao XJ, Yu Q, Ji ZY, Lv YY, Cao Y, Tang CJ, et al. A comparative study of different doped metal cations on the reduction, adsorption and activity of CuO/$Ce_{0.67}M_{0.33}O_2$ (M=Zr^{4+}, Sn^{4+}, Ti^{4+}) catalysts for NO+CO reaction. *Appl Catal, B*. 2013;130–131:293.
46. Cheng K, Liu B, Song WY, Liu J, Chen YS, Zhao Z, et al. Effect of Nb promoter on the structure and performance of iron titanate catalysts for the selective catalytic reduction of NO with NH_3. *Ind Eng Chem Res*. 2018;57:7802.